Environmental Science & Technology

Article

pubs.acs.org/est

Current Magnitude and Mechanisms of Groundwater Discharge in the Arctic: Case Study from Alaska

Natasha T. Dimova,[*,†,‡] Adina Paytan,[‡] John D. Kessler,[§] Katy J. Sparrow,[§] Fenix Garcia-Tigreros Kodovska,[§] Alanna L. Lecher,[‡,∥] Joseph Murray,[‡,⊥] and Slawomir M. Tulaczyk[∥]

[†]Department of Geological Sciences, University of Alabama, Tuscaloosa, Alabama 35487, United States

[‡]Institute of Marine Science, [∥]Department of Earth and Planetary Sciences, and [⊥]Department of Ocean Sciences, University of California Santa Cruz, Santa Cruz, California 95064, United States

[§]Department of Earth and Environmental Sciences, University of Rochester, Rochester, New York 14627, United States

Supporting Information

ABSTRACT: To better understand groundwater−surface water dynamics in high latitude areas, we conducted a field study at three sites in Alaska with varying permafrost coverage. The natural groundwater tracer (^{222}Rn, radon) was used to evaluate groundwater discharge, and electrical resistivity tomography (ERT) was used to examine subsurface mixing dynamics. Different controls govern groundwater discharge at these sites. In areas with sporadic permafrost (Kasitsna Bay), the major driver of submarine groundwater discharge is tidal pumping, due to the large tidal oscillations, whereas at Point Barrow, a site with continuous permafrost and small tidal amplitudes, fluxes are mostly affected by seasonal permafrost thawing. Extended areas of low resistivity in the subsurface alongshore combined with high radon in surface water suggests that groundwater−surface water interactions might enhance heat transport into deeper permafrost layers promoting permafrost thawing, thereby enhancing groundwater discharge.

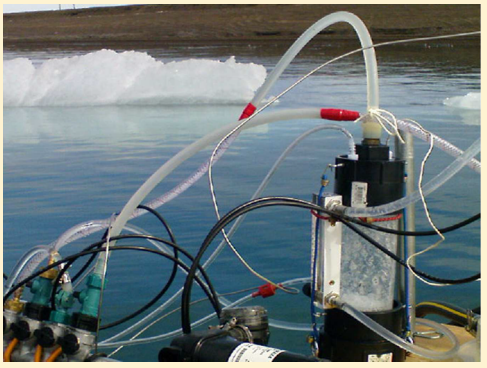

1. INTRODUCTION

Estimating groundwater fluxes into surface bodies of water is difficult because of the large temporal and spatial variability of seepage. In high latitude regions, such as Alaska, quantifying groundwater discharge is even more challenging because of the limited hydrogeological data and extreme changes in aquifer permeability on a seasonal basis.[1−3] The few previous estimates of groundwater discharge in the Arctic include large uncertainties mostly due to unknown aquifer properties.[4−7] While on a geological time scale groundwater dynamics are governed mostly (but not exclusively) by climate and sea level fluctuations, on a shorter time scale, mechanisms of groundwater discharge and magnitude in high latitudes are strongly influenced by the seasonal status of permafrost.[8] Current and future increases in global annual temperatures are expected to substantially remodel the Arctic aquifer architecture and thus its associated groundwater fluxes.[9]

The aquifers of Alaska have never been mapped in detail, except in the immediate vicinity of more-populated areas.[2] Coarse-grained alluvial and glacial outwash deposits of Quaternary age are present in many of the lowlands and are considered the principal groundwater aquifer for populated areas such as Fairbanks and Anchorage. In the northern part of the zone of continuous permafrost, from the Brooks Range northward to the Arctic Ocean, the alluvial and outwash deposits are frozen during most of the year and exploration for local sources of groundwater has not been systematically conducted.

As a result, our current understanding of groundwater dynamics in the Arctic is based mostly on either numerical simulations[9,10] or modeling of regional groundwater flow systems in places where some knowledge of subsurface hydrogeology exists.[1,3,5,11] In all cases, the limited information about these aquifer systems requires assumptions concerning aquifer properties that result in large uncertainties of the final estimates.[7] In this study, we used a radon-based field tracer technique to quantify groundwater fluxes into two coastal sites, one in the North Pacific and a second in the Arctic Ocean, as well as a kettle lake at the foothills of the Brooks Range. The radon tracer approach does not require direct knowledge of aquifer or permafrost properties, a significant advantage for studying groundwater discharge in areas dominated by a frozen groundwater table during most of the year. We define groundwater discharge as the total subsurface flow of water into open water bodies, which includes (but is not limited to) the following: (i) topographically driven fresh groundwater outflow, (ii) fluids released from permafrost degradation, and

Received: May 5, 2015
Revised: September 2, 2015
Accepted: September 15, 2015

DOI: 10.1021/acs.est.5b02215
Environ. Sci. Technol. XXXX, XXX, XXX−XXX

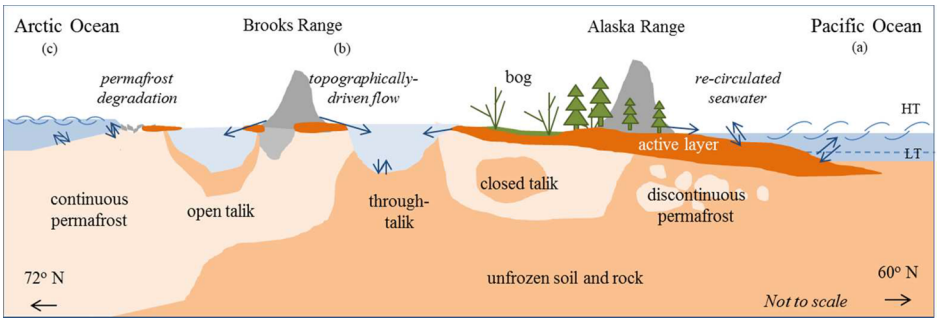

Figure 1. Conceptual south–north cross section of Alaska indicating the three research areas of this study. From south to north these sites include the following: (a) North Pacific coastline (Kasitsna Bay, Seldovia Slough), (b) Brooks Range (Toolik Lake), and (c) Arctic coastline (Point Barrow). The active layer (orange color) is thinning from south to north, while the percentage of permafrost coverage (tan color) increases in the same direction. Arrows indicate areas of groundwater–surface water interactions depicting dominant discharge mechanisms. "HT" and "LT" refer to high and low tide and emphasize the significance of tidal pumping as the main driving force for submarine groundwater discharge on the North Pacific coastline. This is in contrast to the other two sites with topographically driven flow and meltwater fed flow from permafrost degradation.

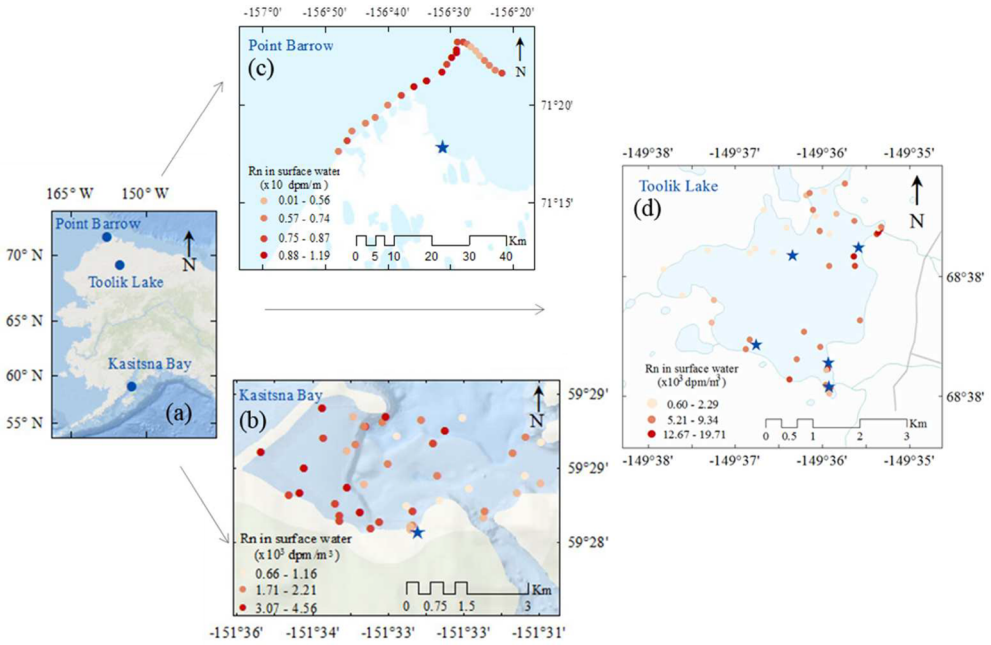

Figure 2. Alaska map (a) showing the locations of the study sites (blue dots). Maps in the middle and right panels display radon concentrations in surface water of the three research sites: Kasitsna Bay (b), Point Barrow (c), and Toolik Lake (d). Stars on each individual site map indicate the locations of the continuous radon time-series deployments.

(iii) recirculated seawater due to tidal pumping and wave setup in coastal areas (Figure 1). This intentionally given liberal definition of the term "groundwater" is in agreement with an established conceptualization of submarine groundwater discharge (SGD), and it allows for comparison between areas with contrasting hydrogeologic, morphologic, and climatic regimes.[12,13] SGD at depths >100 m associated with offshore submarine seepage and generated by density gradients resulting from thermal expansion and salinity differences, as studied by Deming et al.,[11] is not considered here because most of the sampling during this study was performed in near-shore areas. To our knowledge, this is the first field study using a radon tracing approach attempting to assess groundwater discharge for extended areas with contrasting permafrost coverage during "flow conditions". During winter most of the subsurface in the Arctic is frozen and groundwater flow is very limited or zero. We thus herein refer to "flow season", the summer months of thawed subsurface, and "nonflow season", the winter.

2. STUDY SITES AND METHODS

The effect of permafrost on SGD fluxes and mechanisms of discharge were studied at the shorelines of three sites in Alaska (Figure 1 and 2a). From south to north, with increasing permafrost thickness and percent areal coverage, the examined sites include Kasitsna Bay and Seldovia Slough (North Pacific, 0% permafrost coverage), Toolik Lake (foothill of Brooks Range, 50–90% coverage), and two coastal sites within the Arctic Coastal Plain (Kasitsna Bay and Seldovia Slough), the Beaufort Sea (Point Barrow) and Elson Lagoon (>90% coverage)[14,15] (Figure 2). Sources of radon to the water column include groundwater discharge, diffusion from sediments, and production from dissolved ^{226}Ra (direct radon parent), whereas losses accounted for in the model are results of gas evasion, radioactive decay, and mixing with offshore radon-depleted water in the case of tidally influenced coastal sites (Figure 3). Surface water concentrations presented here are corrected for Rn gas evasion using a model suggested in ref

DOI: 10.1021/acs.est.5b02215
Environ. Sci. Technol. XXXX, XXX, XXX–XXX

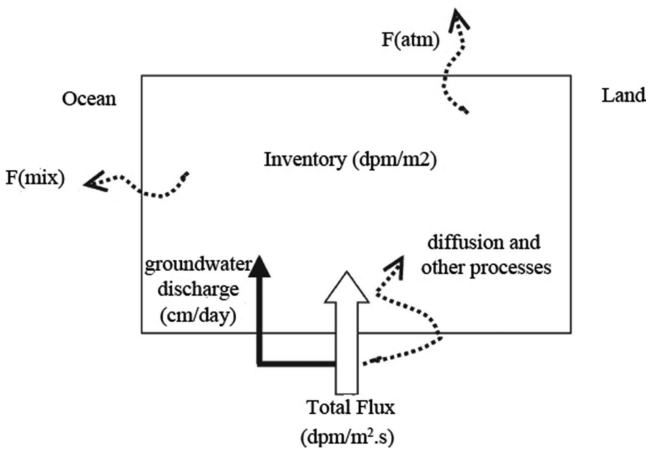

Figure 3. Radon mass-balance box model describing all sources and sinks in case of non-steady-state scenario (i.e., tidally influenced coastal sites) which includes the following: (1) total benthic fluxes via submarine groundwater discharge (SGD) and (2) diffusion from sediments; (3) production from dissolved ^{226}Ra (direct radon parent). Radon losses are results of (1) gas evasion, (2) radioactive decay, and (3) mixing with offshore radon-depleted water. The last sink is typical only for tidally affected coastal environments. In all cases, the excess inventory per time (i.e., differences between sources and sinks fluxes) are divided by radon concentration in groundwater (i.e., groundwater end member) to calculate groundwater discharge. Adapted with permission from ref 22. Copyright 2003 Elsevier.

16 that has been recently verified both for marine environments in ref 17 and for lakes in ref 18. Diffusive flux experiments incubating ~150−200 g of soil in a gastight Erlenmeyer flask as described in refs 19 and 20 were performed with sediments from the active layers from each site. However, the laboratory-measured diffusive fluxes were below 1% compared to the net excess radon delivered by advective groundwater discharge. Therefore, these were neglected in the total radon balance. In the case of surface water inputs such as small creeks and inlets, the radon model takes into account total delivered radon to the system (mass-balance box), regardless if it is entrained via direct seepage on the shorelines or enters the lake as stream's groundwater base flow. We follow the definition for "net excess radon" in ref 21 as the net difference inventories between all radon sources and sinks. The main assumption in this tracer approach is that the input of radon to the overlying surface waters is the dominant source which was indeed the case for this study at all sites. Radon mass-balance models were used to evaluate discharge and were adapted for each site. In the tidally influenced coastal site at the North Pacific site, we used a non-steady-state approach. Radon inventories in the water column were calculated over 30 min intervals, and excess radon delivered by SGD was evaluated by the difference between two consecutive measurements.[22] To calculate discharge in Toolik Lake and in Elson Lagoon (Arctic Ocean), we used a steady-state model developed by Cable et al.[21] and further refined by Dimova and Burnett[18] where excess average radon delivered via groundwater was calculated by balancing observed radon

Table 1. Model Parameters for All Study Sites

research site ID	^{222}Rn in sw × 10^3 (dpm m^{-3})	^{222}Rn in gw × 10^3 (dpm m^{-3})	^{226}Ra (dpm 100 L^{-1})	av water depth (m)	wind speed (m s^{-1})	sp cond (mSv cm^{-1})	GW flux (cm day^{-1})
			North Pacific Coast				
			2011				
Seldovia Slough	2.96 ± 1.0	66.5 ± 6.7	12.5 ± 2.0	5.3 ± 1.7	0.56 ± 1.0	46.7 ± 0.4	170 ± 240
	n = 99	*n* = 19	*n* = 1	*n* = 99	*n* = 99	*n* = 99	*n* = 97
		24.9 ± 2.1					
		n = 3					
			2012				
NOAA dock 1	1.92 ± 0.6	42.1 ± 6.2	12.5 ± 2.0	7.8 ± 5.3	1.6 ± 1.5	n/a	260 ± 360
	n = 150	*n* = 72	*n* = 1	*n* = 152	*n* = 152		*n* = 149
NOAA dock 2	1.20 ± 0.3	42.1 ± 6.2	12.5 ± 2.0	7.95 ± 5.0	1.6 ± 1.5	47.6 ± 0.2	130 ± 180
	n = 146	*n* = 72	*n* = 1	*n* = 148	*n* = 152	*n* = 251	*n* = 145
			Toolik Lake				
			2011				
east dock	5.94 ± 1.1	411 ± 2	0.87 ± 0.2	1.8	3.1 ± 0.9	n/a	1.2
	n = 95	*n* = 3	*n* = 1		*n* = 95		
NE boat	1.92 ± 0.2	411 ± 2	0.87 ± 0.2	1.8	2.8 ± 0.9	n/a	0.6
	n = 50	*n* = 3	*n* = 1		*n* = 50		
SE boat	10.1 ± 2.8	411 ± 2	0.87 ± 0.2	1.8	3.8 ± 1.9	n/a	2.3
	n = 54	*n* = 3	*n* = 1		*n* = 54		
			2012				
east dock	4.26 ± 1.1	314 ± 6	0.87 ± 0.2	1.8	2.8 ± 1.3	n/a	1.5
	n = 209	*n* = 3	*n* = 1		*n* = 222		
midlake	1.16 ± 0.3	314 ± 6	0.87 ± 0.2	1.8	2.8 ± 1.3	n/a	0.8
	n = 102	*n* = 3	*n* = 1		*n* = 222		
			Arctic Ocean Coastline				
			2012				
Elson Lagoon	1.10 ± 0.6	79.1 ± 4	35.6 ± 5.8	2.4	3.8 ± 0.9	23.3 ± 4.9	0.8 ± 0.4
	n = 21	*n* = 10	*n* = 1		*n* = 5	*n* = 109	
Beaufort Sea	0.80 ± 0.2	62.1 ± 1.2	12.2 ± 2.0	2.5	3.3 ± 1.2	27.3 ± 0.9	1.2 ± 0.5
	n = 25	*n* = 7	*n* = 1		*n* = 35	*n* = 238	

DOI: 10.1021/acs.est.5b02215
Environ. Sci. Technol. XXXX, XXX, XXX−XXX

inventories in the water column against atmospheric and decay losses to obtain fluxes. Along the coastline of the Beaufort Sea where strong winds did not allow long-term instrumentation deployment, we used data from a daily survey and constructed a mass balance similar to ref 23. Groundwater discharge in all scenarios was calculated by dividing the net excess radon fluxes by site-specific radon concentrations in the local groundwater (i.e., groundwater end member). At each research site, radon concentrations in groundwater were evaluated for each specific field campaign using continuous radon measurements of pit/groundwater (Seldovia Slough, Kasitsna Bay, Beaufort Sea, and Elson Lagoon) or well groundwater (Toolik Lake). Reported radon concentrations in groundwater are averages ($\pm 1\sigma$) of several consecutive measurements after the system reached full gas/radioactive equilibrium (Figures S7−S10). These fluids were considered representative of the discharging groundwater. Dissolved ^{226}Ra (direct parent of ^{222}Rn) in surface waters was assessed using procedure described by Geibert et al.[24] Reported uncertainties of the advection rates are based on averages of several deployments (usually two or three) and thus reflect both temporal and spatial variability within each specific study area. All field data used for constructing the models are reported in the Supporting Information (Figures S1−S15) and summarized in Table 1.

Spatial distribution and preferential flows were examined via continuous measurements of radon/conductivity/salinity (10 min intervals) in boat surveys at Kasitsna Bay and Toolik Lake during two consecutive years (2011 and 2012), as well as along the Arctic Ocean coastline in the Beaufort Sea in 2012 (Figure 2 and Table 1). To assist our tracer observations and to gain a better understanding of preferential flow paths and mechanisms of discharge, electrical resistivity tomography (ERT) images from shallow depths (up to 15 m below surface soil) were acquired at all sites. Because measured resistivity is largely controlled by the electrolytic conduction of the subsurface waters, ERT measurements can provide information on the relative distribution of ice and water in the liquid state. High resistivity values (up to 1×10^5 ohm·m) were associated with permafrost, whereas values below 200 ohm·m were associated with meltwater and between 0.1 and 1 ohm·m were associated with salt/brackish water. For identifying the interface between the top active layer (meltwater) and permafrost (ground ice), we used values reported in ref 25. Additional verification was done by digging shallow pits at the study sites. ERT arrays in Toolik Lake were positioned across surface water with the end of the cable partially under water (<20 cm) (lake or stream, Figure 4b−d). To improve the precision of inversion of the underwater sections, inverse in situ surface water conductivity measurements ($1/C$) were used in the inversion process. Topographic correction was required only for the array that was deployed shore-perpendicular to Toolik Lake. In this case the vertical axis is reported in elevation instead of depth below surface (Figure 4b). Multiple repeated runs from Wenner and/or dipole−dipole arrays at single locations were combined using Earth Imager (AGI) to achieve high resolution and reduce the absolute error of inversion (which was always <3%, except in Elson Lagoon near Point Barrow).[26] For all coastal sites, the ERT data presented here were collected only during ebb tide when the coastal aquifer is submerged with seawater and the contrast between freshwater and seawater is the most pronounced.

3. RESULTS

The radon tracer data presented here are from detailed daily radon surveys and time-series moorings at multiple sites at each of the studied locations (Table 1). At the North Pacific coast, an area with no or sporadic permafrost coverage, radon concentrations in the surface waters of both Seldovia Slough and Kasitsna Bay were relatively low (average $(2.0 \pm 0.9) \times 10^3$ dpm m^{-3}) (Table 1) when compared to radon concentrations from coastal areas with temperate climate and year-long groundwater flowing conditions.[18,21] In Kasitsna Bay, on average, the radon concentrations in the surface water were slightly higher, $(1.65 \pm 0.6) \times 10^3$ dpm m^{-3}, than those in the 5 m deep water layer, $(1.08 \pm 0.2) \times 10^3$ dpm m^{-3}. Higher radon concentrations were observed closer to the shore, whereas offshore waters were mostly depleted in radon (Figure 2b). Two continuous 3-day time-series records at the beach face of Kasitsna Bay in the summer of 2012 revealed large variations of radon concentrations in surface water ranging from 0.5×10^3 to 4.2×10^3 dpm m^{-3} (Figures S1A, S2A, and S3A) modulated by the large tidal oscillations, which range from −0.5 to 5.8 m MLLW (mean lower low water) datum (station ID 9455517, NOAA, Kachemak Bay). Despite the large changes in water depth, the specific conductivity records from the NOAA dock 2 mooring and Seldovia Slough at the beach face did not show pronounced variations, on average from 47.2 to 48.0 mSv cm^{-1} (Figures S1A and S3A). Water column profiles of specific conductivity and temperature collected at one of the monitoring stations at NOAA dock 1 revealed also a uniform water column during flood and ebb tides (Figure S13). Because the water profiles at the radon mooring station did not show significant water stratification (Figure S13), we assumed uniform water column and radon inventories were integrated over the entire water column. Applying a non-steady-state radon model,[22] the total SGD fluxes reflected the large tidal variations: SGD fluxes in 2011 in Seldovia Slough were 170 ± 240 cm day^{-1} (n = 97), whereas in 2011 and 2012 in Kasitsna Bay they were 260 ± 360 cm day^{-1} (n = 149) and 130 ± 180 cm day^{-1} (n = 145). Note that the reported variability of each site-specific estimate is based on differences in fluxes of 30 min assessments and it is not a result of analytical measurement uncertainties (Figures S1B, S2B, and S3B). The average total SGD (saline and freshwater) at the North Pacific sites calculated from the three areas is 187 ± 67 cm day^{-1} (n = 3) (Table 1). To evaluate the freshwater component of the SGD at this site, a simple experiment was performed. In a volume constrained pit (~12-L perforated bucket) ~ 200 m inland from the midtide line, we deployed a ceramic conductivity−temperature−depth (CTD) sensor and monitored changes in temperature and conductivity/salinity in pit water during two consecutive falling tides (Figure S15A and 15B). Based on these data and using a two-component mixing equation, we calculated freshwater fluxes between 0.8 and 3.0 cm day^{-1} through the cross section of 0.05 m^2 of the pit. Compared to the average radon-derived discharge rates of 186 ± 67 cm day^{-1}, this is only ~1% of the total SGD to Kasitsna Bay. This finding is well supported by the relatively small conductivity variations in surface bay water measured during the time-series deployments (Figures S1A and S3A). Resistivity profiles from several combined shore-parallel arrays at the beach face at Kasitsna Bay in 2012 during ebb tide show a constant resistivity distribution confirming (depth up to 12 m) no indication of the presence of permafrost (Figure 4a).

DOI: 10.1021/acs.est.5b02215
Environ. Sci. Technol. XXXX, XXX, XXX−XXX

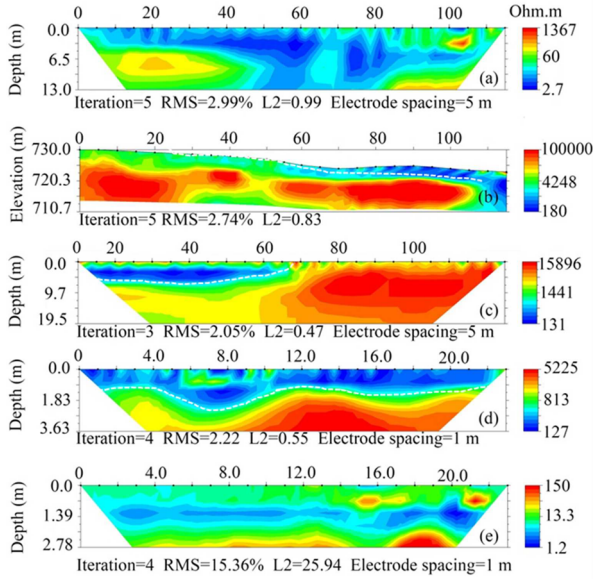

Figure 4. Top image (a) is from a shore-parallel 110 m long array with 5 m spacing at Kasitsna Bay, the research site with sporadic and absent permafrost coverage. Images (b) and (c) were acquired with similar cable configuration at Toolik Lake, the site with discontinuous to continuous permafrost: image (b) was collected with the cable positioned perpendicular to the lake shore over a small elevation on the west side of Toolik, whereas for image (c) the cable was placed across the Kling Inlet. Image (d) was collected with 25 m cable at 1 m spacing parallel to the lake shore and depicts only the active layer. The last image (e) was collected on the shore of Elson Lagoon, near Point Barrow, and the cable was parallel to the shore. This image was also collected with 25 m cable with 1 m spacing, and the goal was to capture active layer structure in this area of thick permafrost coverage.

The average radon concentration in the surface waters of Toolik Lake, obtained from five time-series deployments in 2011 and 2012, was (5.9 ± 4.0) × 10^3 dpm m^{-3} (Table 1). Continuous radon measurements at the mouth of the main river inlet to Toolik Lake, also known as the Kling Inlet, and a smaller creek at the north lake shore showed distinctively higher radon concentrations with averages of (18 ± 2.5) × 10^3 and (14 ± 1.4) × 10^3 dpm m^{-3}, respectively (Figure S12) compared to lake water radon activities. Boat surveys in 2011 and 2012 showed nonuniform radon distributions with higher radon at the inlet areas (Figure 2d). During surveys, water column profiles were performed at five different locations in the lake; all profiles indicated a fairly uniform water column and no significant vertical stratification (Figure S12). Groundwater at Toolik Lake was sampled from a well (65 m deep) near the lake shore, and the radon concentration in groundwater was (411 ± 2) × 10^3 dpm m^{-3} in 2011 and (314 ± 6) × 10^3 dpm m^{-3} in 2012 (Table 1 and Figure S9). Using steady-state ^{222}Rn mass balance calculations,[18] the average groundwater flux to Toolik Lake was 1.4 ± 0.9 cm day^{-1} in 2011 and 1.1 ± 0.5 cm day^{-1}, in year 2012 (Table 1). Note that (i) these estimates are based on different locations each year and (ii) the estimates should be treated as minimum groundwater fluxes given the high radon groundwater end-member used. Extrapolating over the entire lake surface of 1.5 × 10^6 m^2, these estimates yield groundwater discharge of (2.1 ± 1.3) × 10^4 m^3 day^{-1} (2011) and (1.6 ± 0.6) × 10^4 m^3 day^{-1} (2012). Attributed uncertainties to these values are based on average radon concentrations from five moorings deployed around the perimeter of the lake and are thus representative of the observed spatial variability of groundwater discharge to Toolik Lake, not the method's analytical precision. Observed spatial radon heterogeneities prompted us to further explore the areas of preferential groundwater input to the lake. During the summer of 2011, we deployed ERT arrays at three locations in Toolik Lake (Figure 4b–d) and imaged subsurface areas of groundwater/permafrost–surface water interactions along the edges of the lake and a cross section of the Kling Inlet. All three ERT profiles (images up to 15 m depth) revealed lower resistivity values both underneath the main lake inlet (Figure 4c) and close to the lake shore (Figure 4b,d) suggesting unfrozen ice sections.

A >10 km-long radon and salinity boat survey was conducted along the coastline of the Arctic Ocean (Beaufort Sea) near Point Barrow in August 2012 (Figure 2c). At this site, the surface water radon concentrations were consistently low, an average (0.80 ± 0.2) × 10^3 (n = 23) dpm m^{-3} (Table 1). Strong winds up to 9 m s^{-1} (Barrow Airport) during the field sampling period did not allow for time-series deployment of radon instrumentation on the Arctic Ocean coast. To calculate SGD to the Beaufort Sea, we used an average value of radon concentration in surface water obtained from the 6-h radon survey carried out along the shore of Point Barrow. Using excess radon inventories in the uniform water column and the estimated groundwater end member recovered from pit water, the radon mass balance resulted in a groundwater flux of 1.2 ± 0.5 cm day^{-1} (Table 1). The average radon concentration in groundwater from a pit near the Arctic Ocean coast did not show great variations with tide, and was (62 ± 1.2) × 10^3 dpm m^{-3} (n = 7) (Table 1 and Figure S10B). This is in agreement with the low range in tidal amplitude of 0.18–0.37 m, MLLW datum, at this site (station ID 9494935, NOAA, http://tidesandcurrents.noaa.gov/stationhome.html?id=9494935). A comparable result was obtained from two short (2.5–3 h) radon time-series deployments at moorings deployed from a small boat at ∼50 and ∼200 m offshore in Elson Lagoon. Results from these measurements revealed a radon concentration gradient with average radon concentrations of (1.2 ± 0.5) × 10^3 dpm m^{-3} (Figure S6). We attribute this slight excess radon in the near-shore waters to subsurface seepage (perhaps from permafrost degradation) at the Elson Lagoon shore. The wind speed during this deployment was up to 5 m s^{-1}, requiring a rather large correction for atmospheric loss (up to 50%). Concurrent continuous radon concentration measurements in pore fluids recovered at the depth of the permafrost table (∼0.5 m deep pit) on the Elson Lagoon shore did not vary significantly during our measurements and were very similar to the one observed at the shore of the Beaufort Sea, (79.1 ± 4) × 10^3 dpm m^{-3} (n = 10) (Table 1 and Figure S10A). Using this groundwater end member, we found that, in order to maintain the observed excess radon inventory in the water column, there must be a groundwater flux of 0.8 ± 0.4 cm day^{-1}. Expecting a very shallow permafrost table at this site of continuous thick permafrost, we used a different electrical resistivity setup compared to the other two research sites. ERT arrays of shorter length (25 m cable) with 1 m spacing in Wenner's mode allowed us to obtain shallow images of only the active layer (hence the low resistivity values observed) but to achieve higher lateral resolution. Low resistivity values correspond with melted ice up to 1.4 m depth (Figure 3e).[25]

DOI: 10.1021/acs.est.5b02215
Environ. Sci. Technol. XXXX, XXX, XXX–XXX

Table 2. Suggested Driving Forces of SGD in the Arctic

study area	permafrost coverage (%)	dominant groundwater driving force	av specific discharge (cm day^{-1})
North Pacific	>0−10	**marine**	187 ± 67
	absent and isolated	− tidal pumping	(99% marine)
inland kettle lake	50−90	**terrestrial**	1.25 ± 1.15
	discontinuous and continuous	− hydraulic gradients	
		− surface runoff enforcement	(100% fresh)
Arctic Ocean		**glacial/marine**	1.0 ± 0.3
	>90	− permafrost melting	
	thick and continuous	− wave setup	(brackish)

4. DISCUSSION AND CONCLUSIONS

The results of this study reveal detectable fluxes of SGD at all three sites in Alaska. These fluxes should be interpreted as total subsurface flow regardless of the fluids' composition and mechanisms of discharge (see our definition in the Introduction). However, the observed patterns of the radon and salinity tracers in the surface waters during time-series and spatial surveys in receiving waters at these three representative settings suggests different driving mechanisms (Table 2) that were also confirmed by ERT subsurface images. At Kasitsna Bay, an area with high topographic gradients at the North Pacific coast (Figure 1), one would expect primarily gravity-driven subsurface flow. However, time-series deployments at the beach face showed small conductivity/salinity variations with tide and our salinity mass balance indicates that only 1% of the SGD in the area is fresh. Thus, based on the observed large tidal variations (up to 6 m during spring tide), we conclude that almost all of the SGD at this site is composed of recirculated fluids (close to seawater in composition) that enter the aquifer due to marine forcing and only 1% of the discharge is topographically driven terrestrial fresh groundwater. The tidal fluctuations result in unique bay water circulation: freshwater inputs (surface water and groundwater) released during ebb tide result in a stratified water column with a fresher layer (<5 m) on the surface that is exported offshore. During flood tide, the same water is pushed back into the bay resulting in a relatively well-mixed surface water column. This vigorous mixing of coastal waters with radon-depleted water has resulted in the observed low radon concentrations in Kasitsna Bay, which is part of a large fjord system (with an average depth of ∼40 m, http://www.nauticalcharts.noaa.gov/). Using a combined approach of water chemistry analyses and water mass-balance models to evaluate groundwater recharge to perched-precipitation ponds in areas of the Kenai Peninsula (Cook Inlet) during the summer of 2006[5] found similar freshwater seepage rates, 0.82 (±1.12) and 2.78 cm day^{-1}.[5] Assessments were based on seven on-land ponds and are equivalent to our on-land gravity-driven fresh groundwater flux salinity balance assessments. The hydraulic connection of the coastal aquifer system with the ocean at this site appeared to be the most pronounced of those investigated. The large discharge per unit area, 186 ± 64 cm/day, the highest measured in this study, was facilitated by low (or even absent) permafrost coverage and a large tidal range. Fluxes of similar magnitude (85 ± 84 cm day^{-1}) were previously reported in a smaller scale fjord system in Hood Canal, WA, by Swarzenski et al.[27] These large SGD values are a result of the large volume of lateral seawater exchange of the coastal aquifer and are mostly saline in nature (e.g., recirculated seawater driven by tides). None-point diffusive groundwater fluxes were confirmed by ERT images (Figure 4a); resistivity distribution did not indicate preferential seawater flows. These discharge rates are also of the same order of magnitude as radium based SGD fluxes at this site.[28] During our sampling campaigns, we observed massive inundation of the North Pacific coastal areas during flood tide and subsequent "land-draining" during ebb tide. Such diurnal flooding events create a mechanism for mobilization of land-born contaminants and facilitate constituent (nutrients, organic matter, etc.) fluxes to the ocean. We foresee that, with continuing climate warming and rising sea level trends, coastal permafrost erosion will progress and ultimately result in increased saltwater intrusion into the aquifers of these and similar coastal areas.

We did not find large differences in the groundwater discharge to Toolik Lake over two consecutive years ((2.1 ± 1.3) × 10^4 and (1.6 ± 0.6) × 10^4 m^3 day^{-1}). These fluxes are comparable in magnitude to the groundwater discharge estimate (3.64 × 10^4 m^3 day^{-1}) from a water balance by Whalen and Cornwell[29] and recently published data by Paytan et al.[30] based on a radium mass balance. The findings in this study indicate that groundwater discharge into Toolik Lake is likely determined by a combination of (i) gravity-driven flow (a result of the high topography in the area) and (ii) meltwater released from thawing permafrost. While we cannot, at this point, distinguish which process is dominant, a few findings here give us more insights than previously known. First, the spatial radon distribution (Figure 2d) clearly shows that elevated radon areas of the lake are not associated with higher topographic gradients in the northwest and west. In contrast, high radon is observed along the areas of surface runoff (Figure 2d). Furthermore, high radon concentrations in surface waters around these areas (indication for larger groundwater inputs) were also confirmed by resistivity anomalies (low resistivity) in the active layer detected in both shore-perpendicular and shore-parallel ERT arrays (Figure 4b−d). We attribute these extended unfrozen areas to permafrost degradation that results from permafrost (frozen groundwater)−surface water interactions. We argue that wave-forcing at the lake shore and surface water runoff promotes heat advection in deeper subsurface layers during the summer expending of the hyporheic zone (low resistivity zone between the permafrost table (white dashed line) and cable (top black line) in Figures 2b−d) that ultimately results in higher groundwater discharge. Similar effects of enhanced groundwater flow and storage in areas of surface runoff were reported in ref 31 for the watershed of the Yangtze River. Using data for average stream velocity from the LTERNET Database for September 2009 (the closest time to our sampling campaign in 2012), we calculated that at an average monthly stream stage of 0.4 ± 0.06 m, a discharge of

DOI: 10.1021/acs.est.5b02215
Environ. Sci. Technol. XXXX, XXX, XXX−XXX

0.4 ± 0.4 m s^{-1}, a cross section at the inlet mouth of 2.08 m, and radon inlet inventories of 7500 dpm m^{-2} from our time series (Figures S11 and 12), the radon flux to the lake from the inlet is approximately 1300 dpm m^{-2} day^{-1}. Compared to the total groundwater-derived radon flux of 4700 dpm m^{-2} day^{-1} based on our steady-state lake model, the river input is about 30% of the total radon inventories in Toolik Lake.

ERT large-scale offshore profiles and borehole data reported by Overduin et al.[32] have shown that thick submarine ice covers large parts of the Arctic Ocean continental shelf extending to about 900 m offshore. The thick permafrost layer in these Arctic areas acts as a barrier, preventing both recharge and discharge into the aquifer. Furthermore, this physical boundary also results in limited contact between the permafrost table and the underlying bedrock and ultimately is expected to result in lower radon activities in the permafrost meltwater. Indeed, the radon concentrations in offshore waters and pit/groundwater at Point Barrow were the lowest measured during this study (Table 1). A uniform radon concentration across the sampled groundwater (spatially and temporally) suggests a single source. We argue that this source is most likely meltwater that originates from submarine or shallow degraded coastal permafrost that covers the entire area. The similarity of the radon activity values in groundwater at Elson Lagoon shore ($(79 \pm 4) \times 10^3$ dpm m^{-3}) and the Beaufort Sea coastal site ($(62 \pm 1.2) \times 10^3$ dpm m^{-3}) also suggests a common end member, i.e., meltwater. Recently published stable isotopes analyzes by Lecher et al.[28] from the same area are consistent with this hypothesis. Small variations of radon concentrations in pit water suggest that tidal pumping is not the main driving force at this coastal area (Table 1). Indeed, the tidal range at Point Barrow is negligible (0.18−0.37 m) and we assume the range in the Elson Lagoon (semienclosed coastal lagoon) must be even smaller. A terrestrial driving mechanism (i.e., gravity-driven flow) is also excluded as a possibility due to the flat regional topography; the coastal plain is only at ∼60 cm above sea level. Our ERT arrays did not show preferential flows of groundwater (Figure 4e). The groundwater flux determined by the radon mass-balance model indicates a discharge of 1.2 ± 0.5 cm day^{-1} at the Beaufort Sea coastline. This value is of the same order as at Toolik Lake (1.1 and 1.4 cm day^{-1}) and the fresh component of the SGD at Kasitsna Bay (1.94 cm day^{-1}). However, the uncertainties associated with the calculations at the Barrow sites are larger because (i) our radon mass balance is based on a relatively short time-series record (Elson Lagoon) and (ii) the radon activities in surface water were the lowest measured during this study and thus had the highest analytical measurement errors (Table 1).

The aim of this work was to assess and compare SGD fluxes and mechanisms of discharge in Arctic areas with contrasting permafrost extent. Although the work presented here is regional (from only three sites in Alaska), it illustrates general scenarios of groundwater−surface water−permafrost interactions that should be typical of similar settings elsewhere in the Arctic. Due to the very limited knowledge of the aquifer systems in permafrost areas, the results here are unique and thus may be used as a baseline of the current magnitude of groundwater discharge in the Arctic in the face of changing climate. With predicted future increases in regional climate variability, these findings have implications for the role of groundwater discharge and constituent budgets (e.g., greenhouse gases, nutrients, organic material) in regional and larger scale terrestrial and marine ecosystems. From a methodological perspective, the radon tracer approach for evaluating SGD was found to be a suitable tool for studying groundwater dynamics in areas of permafrost coverage. Furthermore, due to the similarities in methodology with studies performed elsewhere, assessments herein can be used for comparison purposes and to assemble global SGD flux estimates.

■ ASSOCIATED CONTENT

Supporting Information

The Supporting Information is available free of charge on the ACS Publications website at DOI: 10.1021/acs.est.5b02215.

The Supplementary Information provides the original data used for the construction of the Rn mass balance models in the manuscript. Data of Rn temporal variations (time-series) of surface and groundwater at the different study sites are also presented. Salinity/conductivity profiles used to support the assumption in the Rn groundwater model, is available for all sites as well (PDF)

■ AUTHOR INFORMATION

Corresponding Author

*Phone: 205-348-0256; e-mail: ntdimova@as.ua.edu.

Notes

The authors declare no competing financial interest.

■ ACKNOWLEDGMENTS

This project was funded by the National Science Foundation through grants OCE-1139203 to S.A. Yvon-Lewis and J.D. Kessler, PLR-1417149 to J.D. Kessler, and ARC-1114485 to A. Paytan. This work was also supported by a Sloan Research Fellowship in Ocean Sciences to J.D. Kessler. Technical support was provided by the NOAA and UAF Kasitsna Bay Laboratory, Naval Arctic Research Laboratory, and NSF Polar Field Services. Scientific support was provided by the NOAA and UAF Kasitsna Bay Laboratory and the Naval Arctic Research Laboratory. We thank for the enthusiasm and support of the staff at the Toolik Lake field station and Kasitsna Bay Laboratory.

■ REFERENCES

(1) Bense, V. F.; Kooi, H.; Ferguson, G.; Read, T. Permafrost degradation as a control on hydrogeological regime shifts in a warming climate. *J. Geophys. Res.* **2012**, *117*, F03036.

(2) Callegary, J. B.; Kikuchi, C. P.; Koch, J. C.; Lilly, M. R.; Leake, S. A. Review: Groundwater in Alaska (USA). *Hydrogeol. J.* **2013**, *21*, 25−39.

(3) French, H. *The Periglacial Environment*, 3rd ed.; Wiley: Hoboken, NJ, 2007; 478 pp.

(4) Moore, R. D.; Hamilton, A. S.; Scibek, J. Winter streamflow variability, Yukon Territory, Canada. *Hydrol. Processes* **2002**, *16*, 763−778.

(5) Rains, M. C. Water resources and hydrodynamics of closed-basin depressions, Cook Inlet region, Alaska. *Wetlands* **2011**, *31*, 377−387.

(6) Walvoord, M. A.; Striegl, R. G. Increased groundwater to stream discharge from permafrost thawing in the Yukon River basin: Potential impacts on lateral export of carbon and nitrogen. *Geophys. Res. Lett.* **2007**, *34*, L12402.

(7) Kane, D. L.; Yoshikawa, K.; McNamara, J. P. Regional groundwater flow in an area mapped as continuous permafrost, NE Alaska (USA). *Hydrogeol. J.* **2013**, *21*, 41−52.

(8) Haselwimmer, C.; Prakash, A.; Holdmann, G. Quantifying the heat flux and outflow rate of hot springs using airborne thermal imagery: case study from Pilgrim Hot Springs, Alaska. *Remote Sens. Environ.* **2013**, *136*, 37−46.

DOI: 10.1021/acs.est.5b02215
Environ. Sci. Technol. XXXX, XXX, XXX−XXX

(9) Frampton, A.; Painter, S. L.; Destouni, G. Permafrost degradation and subsurface-flow changes caused by surface warming trends. *Hydrogeol. J.* **2013**, *21*, 271−280.
(10) Bense, V. F.; Ferguson, G.; Kooi, H. Evolution of shallow groundwater flow systems in areas of degrading permafrost. *Geophys. Res. Lett.* **2009**, *36*, L22401.
(11) Deming, D.; Sass, J. H.; Lachenbruch, A. H.; De Rito, R. B. Heat flow and subsurface temperature as evidence for basin-scale groundwater flow, North Slope of Alaska. *Geol. Soc. Am. Bull.* **1992**, *104*, 528−542.
(12) Burnett, W. C.; et al. Groundwater and pore water inputs to the coastal zone. *Biogeochemistry* **2003**, *66*, 3−33.
(13) Moore, W. S. The effect of submarine groundwater discharge on the ocean. *Annu. Rev. Mar. Sci.* **2010**, *2*, 59−88.
(14) Eisner, W. R.; Bockheim, J. G.; Hinkel, K. M.; Brown, T. A.; Nelson, F. E.; Peterson, K. M.; Jones, B. M. Paleoenvironmental analyses of an organic deposit from an erosional landscape remnant, Arctic Coastal Plain of Alaska. *Palaeogeogr., Palaeoclimatol., Palaeoecol.* **2005**, *217*, 187−204.
(15) Wahrhaftig, C. Physiographic divisions of Alaska. *U. S. Geol. Surv. Prof. Pap.* **1965**, *482*, 52.
(16) MacIntyre, S.; Wannikhof, R.; Chanton, J. P. Trace gas exchange across the air-water interface in freshwater and coastal marine environments. In *Biogenic Trace Gases: Measuring Emissions from Soil and Water*; Matson, P. A., Hariss, R. C., Eds.; Blackwell Science: Cambridge, MA, 1995; pp 52−57.
(17) Dulaiova, H.; Burnett, W. C. Radon loss across the water-air interface (Gulf of Thailand) estimated experimentally from ^{222}Rn-^{224}Ra. *Geophys. Res. Lett.* **2006**, *33*, L05606.
(18) Dimova, N. T.; Burnett, W. C. Evaluation of groundwater discharge into small lakes based on the temporal distribution of radon-222. *Limnol. Oceanogr.* **2011**, *56*, 486−494.
(19) Corbett, D. R.; Burnett, W. C.; Cable, P. H.; Clark, S. B. Radon tracing of groundwater input into Par Pond, Savannah River Site. *J. Hydrol.* **1997**, *203*, 209−227.
(20) Martens, C. S.; Kipphut, G. W.; Klump, Y. V. Sediment-water chemical exchange in the coastal zone traced by in situ radon-222 flux measurements. *Science* **1980**, *208*, 285−288.
(21) Cable, J. E.; Burnett, W. C.; Chanton, J. P.; Weatherly, G. L. Estimating groundwater discharge into the northeastern Gulf of Mexico using radon-222. *Earth Planet. Sci. Lett.* **1996**, *144*, 591−604.
(22) Burnett, W. C.; Dulaiova, H. Estimating the dynamics of groundwater input into the coastal zone via continuous radon-222 measurements. *J. Environ. Radioact.* **2003**, *69*, 21−35.
(23) Dulaiova, H.; Camilli, R.; Henderson, P. B.; Charette, M. A. Coupled radon, methane, and nitrate sensors for large-scale assessment of groundwater discharge and non-point source pollution to coastal waters. *J. Environ. Radioact.* **2010**, *101*, 553−563.
(24) Geibert, W.; Rodellas, V.; Annett, A.; Van Beek, P.; Garcia-Orellana, J.; Hsieh, Y.-T; Masque, P. ^{226}Ra determination via the rate of ^{222}Rn ingrowth with the Radium Delayed Coincidence Counter (RaDeCC). *Limnol. Oceanogr.: Methods* **2013**, *11* (2013), 594−603.
(25) Palacky, G. V. Resistivity characteristics of geologic targets. *Electromagnetic Methods in Applied Geophysics*; Society of Exploration Geophysicists: Tulsa, OK, 1988; pp 52−129. DOI: 10.1190/1.9781560802631.ch3
(26) Loke, M. H. *Tutorial: 2-D and 3-D Electrical Imaging Surveys*; 2011. www.geoelectrical.com.
(27) Swarzenski, P.; Simonds, F. W.; Paulson, A. J.; Kruse, S.; Reich, C. Geochemical and geophysical examination of submarine groundwater discharge and associated nutrient loading estimates into Lynch Cove, Hood Canal, WA. *Environ. Sci. Technol.* **2007**, *41*, 7022−7029.
(28) Lecher, A. L.; Kessler, J. D.; Sparrow, K. J.; Garcia-Tigreros Kodovska, F.; Dimova, N.; Murray, J.; Tulaczyk, S.; Paytan, A. Methane transport through submarine groundwater discharge to the North Pacific and Arctic Ocean at two Alaskan sites. *Limnol. Oceanogr.* **2015**, DOI: 10.1002/lno.10118.
(29) Whalen, S. C.; Cornwell, J. C. Nitrogen, Phosphorus, and Organic Carbon Cycling in an Arctic lake. *Can. J. Fish. Aquat. Sci.* **1985**, *42*, 797−808.
(30) Paytan, A.; Lecher, A. L.; Dimova, N.; Sparrow, K. J.; Garcia-Tigreros Kodovska, F.; Murray, J.; Tulaczyk, S.; Kessler, J. D. Methane transport from the active layer to lakes in the Arctic using Toolik Lake, Alaska, as a case study. *Proc. Natl. Acad. Sci. U. S. A.* **2015**, *112*, 3636−3640.
(31) Qiu, J. Thawing permafrost reduces river runoff. *Nature* **2012**, DOI: 10.1038/nature.2012.9749.
(32) Overduin, P. P.; Westermann, S.; Yoshikawa, K.; Haberlau, T.; Romanovsky, V.; Wetterich, S. Geoelectric observations of the degradation of nearshore submarine permafrost at Barrow (Alaskan Beaufort Sea). *J. Geophys. Res.* **2012**, *117*, F02004.

DOI: 10.1021/acs.est.5b02215
Environ. Sci. Technol. XXXX, XXX, XXX−XXX